ARTICLE NO. 79-0237R

Fluid-Structure Interaction Dynamics in Aircraft Fuel Tanks

M. A. Ferman* and W. H. Unger†
McDonnell Aircraft Company, McDonnell Douglas Corporation, St. Louis, Mo.

A study has shown that the fuel in contact with the walls of a fuel cavity causes dramatic changes in the vibration characteristics of the walls. These changes are shown to lead to a variety of consequences significantly altered from the dry state in three areas: namely, fatigue, flutter, and response to ballistic impact (hydraulic ram). The principal focus of this paper is the explanation of the fluid-structure interaction mechanism. A combined analytical and experimental approach is used to describe the process. Formative applications of the concepts to fatigue and flutter are shown, and utilization for hydraulic ram is indicated. These suggest significant results which have not been considered previously and which may have a major influence on design approaches.

Nomenclature

a = tank length
b = tank height
BCS = boundary condition solution
c = tank width or damping coefficient
CM = continuity method
dA = incremental area
D = deflection
f = frequency, Hz
M = mass
Q = dynamic pressure parameter
T = differential Eq. solution—time
u = flow velocity in x
v = flow velocity in y
V = general flow velocity
w = flow velocity in z
x = length coordinate
X = differential Eq. solution for x
y = height coordinate
Y = differential Eq. solution for y
z = width coordinate
Z = differential Eq. solution for z
α = mode shape parameter in z
β = decay rate term in x
γ = mode shape parameter in y
δ = deflection
ϵ = strain
ρ = mass density per unit volume
ϕ = mode shapes
ω = oscillatory frequency—rad/s

Introduction

THIS study is an outgrowth of two incidences of structural damage believed to be attributed to fluid-structure interaction. In the first instance, damage was incurred in a standard vibration qualification test of a fuel cell. This was shown to result from overstress at the wetted panel resonance which coincidentally matched the required driving frequency. In the second instance, cracks developed in the skin of a wing during flight. This was traced to a large amplitude flutter-type of response, and was believed to be caused by altered dynamics resulting from fluid contact with the skins. In both cases, the dry conditions were not critical, nor were the wetted critical conditions easily identified. Having developed cursory explanations, a more extensive effort was initiated to isolate and explain the mechanism and to identify applications, so as to improve design approaches.

While there is considerable work in the literature on the general subject of fluid-structure interaction dating back to Lamb's work in 1920,[1] most articles deal with low frequency slosh, circular plates, or annular tanks.[2-5] Hunt[6,7] presents a straightforward finite element approach. Our approach is slanted toward filling the gap of application to aircraft fuel cells and gaining insight into physical effects including fuel depth, container geometry, panel geometry, and mechanical properties.

The key effects we found were sharply lower frequencies; modified coupling between modes of a panel, or of opposed or adjacent panels; only slightly increased damping; and stress amplification compared to the dry state for equivalent excitation. Fluid disturbances created by the oscillations of contacting structural panels are represented by velocity profiles from which kinetic energy is defined. The fluid kinetic energy is used to describe an induced mass that is added to the structural mass in the basic vibration solution. Thus, the reduction of frequency due to fuel contacting the panels is directly described.

A combined analytical/experimental program was undertaken to describe the overall fluid-structure interaction in the most fundamental case—uniform panels configured as individual side or bottom panels, or as opposed parallel sides. Theory was developed for panels with pinned or fixed edges. Experiments were conducted for all three cases for fixed edge panels. Comparisons between theory and experiment were made for the side and bottom panels, and showed good correlation. Comparison of theory and experiment for the opposed panels has not begun.

Approach

Figure 1 shows three areas—fatigue, flutter, and hydraulic ram—where we believe prime applications can be made, and where our formative efforts may provide insight into problems previously not recognized. We are focusing attention on key new ideas reflected in 1) decreased fatigue life of fuel cell walls in environmental vibration due to increased stress; 2) decreased flutter speed due to coupling of fluid-structural effects in panel flutter and coupling of panel, and primary surface flutter due to fluid interaction; and 3) increased fuel cell damage due to ballistic response (hydraulic ram).

Presented as Paper 79-0237 at the AIAA 17th Aerospace Sciences Meeting, New Orleans, La., Jan. 15-17, 1979; submitted Feb. 12, 1979; revision received June 6, 1979.

Index categories: Structural Dynamics; Vibration; Structural Durability (including Fatigue and Fracture).

*Staff Engineer, Structural Dynamics.
†Sr. Engineer, Structural Dynamics.

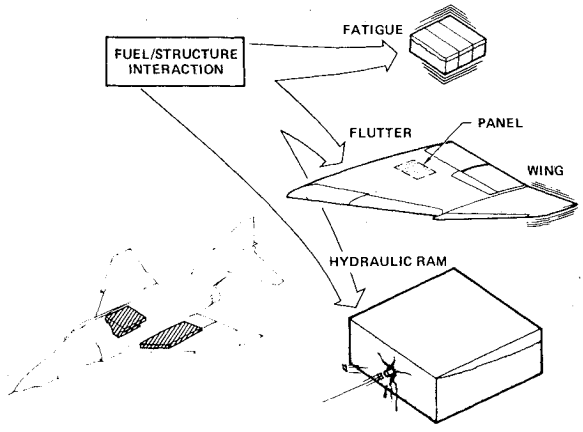

Fig. 1 Applications of fuel/structure interaction.

Each of these three areas features potentially adverse effects attributed to facets of the fuel-structure interaction which are not present in the dry case. In environmental fatigue, the lowered frequencies place panels in regimes of stronger excitation. Larger strains are induced at higher fuel levels. In the panel flutter area, lowered panel frequencies provide a means for added coupling with normally lower structural frequencies. In hydraulic ram, large panel strain intensifications result from the added energy transfer to the fluid and consequently to the panel. Though well known in some regards, panel/fluid coupling has not been fully developed to reflect the mass influence shown here, nor has the additional structural feedback loading suggested here been fully employed.

Interaction Mechanism

As indicated, tank wall oscillations create fluid disturbances that produce mass effects modifying dry panel dynamics. The fluid disturbances are represented by velocity profiles which satisfy Laplace's equation. The velocity profiles provide a means for describing fluid kinetic energy and, hence, mass effects in vibratory equations of motion for the panel/fluid systems. Two basic ideas were used to solve the vibration equations: namely, a Rayleigh-Ritz, or modal approach, and a mini-finite element approach. The former solution was used to gain insight into physical properties, while the latter was investigated as a method offering a broader calculative capability for general use and extension to other configurations.

Rayleigh-Ritz Method

The Rayleigh-Ritz method employs a multi-degree-of-freedom vibration solution expressed in matrix form for an incompressible fluid as

$$[M^P_{JJ}+M^F_{JK}]\{\ddot{\delta}_K\}+[\omega^2_{JJ}M^P_{JJ}]\{\delta_K\}=0 \tag{1}$$

Note that for the case of the incompressible fluid there are no independent freedoms for the fluid, hence no independent fluid mass or stiffness. This was shown in our study and was independently noted previously.[6] Likewise, only small oscillation amplitudes were considered so that linear vibration solution could be used. Here, δ is the panel deflection coordinate, and ω_{JJ} is the circular frequency (rads per sec) of the dry panel in each of the N modes. M^P is the generalized mass of the dry panel expressed as

$$M^P_{JJ}=\int_{\text{panel}}\int \rho_P t_P(\phi^P_J)^2 \mathrm{d}A \tag{2}$$

where ρ_P = panel mass density, t_P is thickness in inches, and $\mathrm{d}A$ is panel incremental area, while ϕ^P_J is the panel mode shape in mode J. Since orthogonal shapes are used, this mass matrix is diagonal.

The fluidic mass term M^F_{JK} is derived from the fluid kinetic energy expression via Lagrange's equation. The fluid velocity profile terms u, v, and w can be symbolized in the following expressions:

$$u=\sum_{K=1}^{N}\phi^u_K(x,y,z)\dot{\delta}_K \tag{3a}$$

$$v=\sum_{K=1}^{N}\phi^v_K(x,y,z)\dot{\delta}_K \tag{3b}$$

$$w=\sum_{K=1}^{N}\phi^w_K(x,y,z)\dot{\delta}_K \tag{3c}$$

where the ϕ terms are analogous to mode shapes for the fluid velocity terms and will be defined below. Substituting Eqs. (3a), (3b), and (3c) into Lagrange's equation and solving for the fluidic generalized mass M^F yields

$$M^F_{JK}=\rho_F\int_{\substack{\text{fluid}\\\text{volume}}}\int\int(\phi^u_J\phi^u_K+\phi^v_J\phi^v_K+\phi^w_J\phi^w_K)\mathrm{d}V \tag{4}$$

where ρ_F is fluid mass density and $\mathrm{d}V$ is the incremental volume.

Panel deflections are computed from the expression shown below, which combines the uncoupled panel shapes with the normal mode ratios of Eq. (1). Specifically the panel deflections D^P in normal mode r are given as

$$D^P_r=\sum_m(\phi^P_m\phi^m_r)\cdot\delta_r \tag{5}$$

where ϕ^P_m are the uncoupled shapes noted earlier, ϕ^m_r are the ratios of the uncoupled δ's expressed in the mode shapes of Eq. (1), and δ_r is the vector used to define ϕ_r.

An IBM 370-195 computer program was developed to solve the vibration equations, mode shapes, and node lines.

Velocity Profiles

Figure 2 shows the geometry of the rectangular tank, coordinate systems, and velocity terms used in this development. The fundamental fluid equations are Euler's equation, the continuity equation, and the irrotationality condition considering an incompressible fluid. These expressions are combined to yield Laplace's equation from which the velocity profiles for u, v, and w are developed. A standard solution to Laplace's equation is to assume a

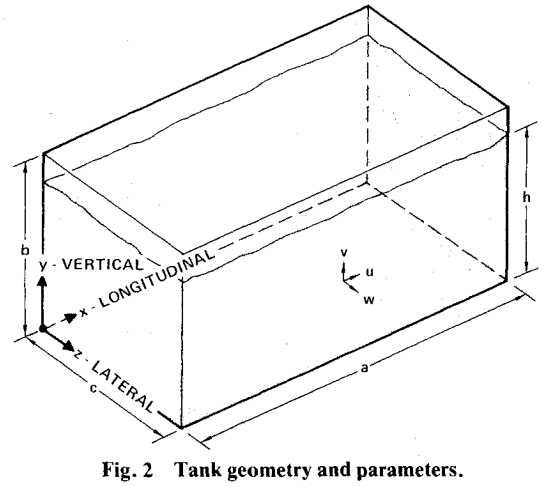

Fig. 2 Tank geometry and parameters.

product form for u, v, and w in terms of x,y,z, and t; for example, for u,

$$u=\sum_m \{[X_u(x)]_m[Y_u(y)]_m[Z_u(z)]_m[T_u(t)]_m\} \quad (6)$$

The time part, $T_u(t)$, is defined to match the panel-related time function since the fluid velocity normal to a panel must equal the panel velocity at the panel. Thus, if an end panel deflection is $X^P=\delta(t)\,F(y,z)$, then $T_u=\dot{\delta}$. Continuing ahead by substituting this relationship for T_u in Eq. (6) and noting separation of variables, we find for pinned panels:

$$Y_u = A_{1u}\cos\gamma y + A_{2u}\sin\gamma y \quad (7a)$$

$$Z_u = B_{1u}\cos\alpha z + B_{2u}\sin\alpha z \quad (7b)$$

$$X_u = C_{1u}e^{+\beta x} + C_{2u}e^{-\beta x}$$

$$\beta^2 = \alpha^2+\gamma^2 \quad (7c)$$

$$T_u = \dot{\delta}$$

The product $X_u\ Y_u\ Z_u$ in Eq. (6) provides the ϕ^u term of Eq. 3(a). Similar equations result for v, w, as would be reflected via $A_{1v}\ldots C_{2v}$ and $A_{1w}\ldots C_{2w}$. It is possible to represent a more general panel shape in a series solution, or merely functionally, as

$$u=[Y(\gamma_m,y)]\,[Z(\alpha_n,z)]\,[\exp(\beta_{mn},x)]\,\dot{\delta} \quad (8)$$

where γ_m and α_n reflect panel modal constants, and the exponential function exp (β_{mn},x) of the form of Eq. (7c) is affected by wave numbers in the other two directions. To keep the solution simple, the fluid velocity normal to, and at, the flexible panel (u in the example) was always chosen to be an elementary function or to be precisely the panel function. Likewise, the relation between β, γ, and α from Eq. (7d) has been maintained.

The solution for v and w, or in general for any of the other two velocities besides the one normal to the flexible panel, can be derived by either satisfying the boundary conditions at the other walls or by reconsidering the particle fluid dynamics. These methods have been used and referred to as 1) the boundary condition solution (BCS) and 2) the continuity method (CM). In the latter method, boundary conditions are also considered but are used to finalize the expressions developed via continuity. Both techniques have been investigated to try to show advantages of one over the other.

Boundary Condition Solution (BCS)

The fluid velocity perpendicular to a flexible wall is set equal to the panel velocity at the flexible wall, and is allowed to diminish (decay exponentially) vs distance from the wall. The analytical form of the other two velocities is determined from the boundary conditions at walls, and flow symmetry in some cases. Velocities normal to rigid walls are zero, while those along rigid walls and at free surfaces are not necessarily zero. The decay rate used on the vector perpendicular to the flexible wall has been used on the other two velocities. Cases of two- and three-dimensional flow are accounted for in the applications.

Continuity Method (CM)

In this method the continuity equations and irrotationality conditions are used to develop two-dimensional (2D) and/or three-dimensional (3D) flow cases. The 2D terms reflect three-dimensional geometry but contain only two flow vectors. In order to separate certain velocity derivatives that create cross influence on each other in 3D flow, the derivatives of the velocity having zero magnitude were also to be treated as zero. In 3D cases, the 2D equivalents for u, v, and w can be directly added, or they can be modified by the cross velocity derivatives to obtain 3D versions.

Little more can be said until examples are given. Thus if a pinned-pinned panel is at the left of the tank in Fig. 2, then u becomes

$$u=\dot{\delta}_{mn}\left(\sin\frac{m\pi y}{b}\sin\frac{n\pi z}{c}\right)\frac{e^{-\beta x}-e^{\beta(x-2a)}}{(1-e^{-2\beta a})} \quad (9a)$$

where

$$\beta=\pi\sqrt{\frac{m^2}{b^2}+\frac{n^2}{c^2}} \quad (9b)$$

Here the sine and exponential terms are the ϕ^u terms of Eq. (3a). The v, w terms can be defined for 2D or 3D flow from eithel the continuity or boundary condition approach. This becomes rather tedious to illustrate in detail. Briefly, however, for 3D flows, the continuity relations for the v term yields

$$v=\dot{\delta}_{mn}\left(\frac{\pi b}{\beta m}\right)\frac{\left(\sin\frac{n\pi z}{c}\right)}{(1-e^{-2\beta a})}\left(1-\cos\frac{m\pi y}{b}\right)$$

$$\cdot\left[\frac{m^2}{b^2}(e^{-\beta x}+e^{+\beta(x-2a)})+\frac{n^2}{c^2}(1+e^{-2\beta a})\right] \quad (10)$$

for $y\le b$.

These equations reflect the influence of container size and geometry on variables, particularly tank length and its effect on the longitudinal decay rate. The sine and cosine functions reflect the height and width, b and c, and describe panel modes for which flows are present in odd or even lobed panel modes. Without digressing into more detail, it can be shown that u and v exist in modes having odd wave numbers in Z, while in 3D flow, u, v, and w would exist in modes having even wave numbers in Z. Usually v is small in 3D cases and thus can be omitted, indicating that u and w are dominant in the even-lobed z modes.

The ideas derived from the study of the flexible side were readily extended to the flexible bottom. The velocity normal to the bottom v was idealized to be similar to u from the side case, i.e., v decays toward the free surface. Likewise, two opposed panels were built up by merging two cases like our original end panel, where two sets of velocity profiles were added by superposition.

Generalized Mass

Formulae for generalized mass can be developed by substituting in Eq. (4) for u, v, w, employing terms as in Eqs. (9) and (10). This becomes extremely complicated using analytical forms. While some of the simple cases were carried out, this became difficult to accomplish accurately and resulted in long expressions that were prone to evaluation errors. We, therefore, resorted to numerical integration processes to eliminate this tedium and source of error. This was added to our computer program.

Mini-Finite Element Method

A mini-finite element method was developed as an alternate means for treating the fluid-structure interaction method. It offers a more general approach. Considerable attention is being given to finite elements of fluids, with some investigators studying the fluid-structure problem.

Hunt[6,7] used pressure and motion connectivity relations in his development to study rectangular tanks. Our approach simplifies the overall complexity through use of a concept borrowed from the Rayleigh method, which we had developed earlier. In this idea, the fluid is treated as containing a series

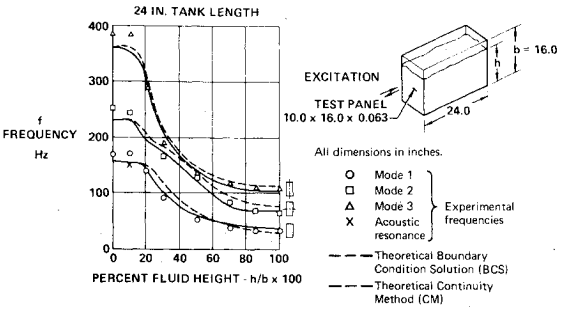

Fig. 3 Comparison of experimental and theoretical frequencies vs fluid height for the flexible end panel.

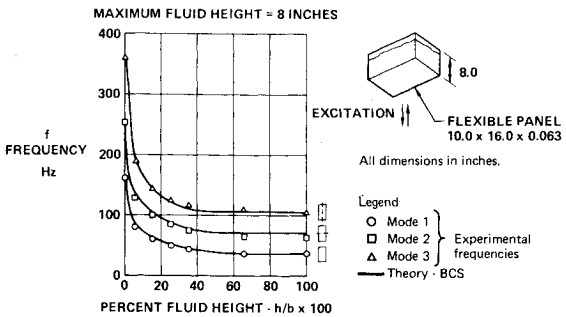

Fig. 4 Comparison of experimental and theoretical frequencies vs fluid height for the flexible bottom panel.

of incremental volumes bounded at one end by an elastic element at the panel of interest and at the other end by a rigid wall or flexible wall, if such exists. Each volume bounds velocity profiles based on the Rayleigh development, i.e., velocities decay to zero as motion progresses away from the flexible panel region. Thus, each volume has kinetic energy values which can be related to the grid point motion surrounding each element. This now allows for fluid inertia loading to be expressed in terms of grid point accelerations, which now combine with the structural grid point masses. The equations are similar in form to Eq. (1), except that grid point mass and stiffness data are used and the solution is a direct calculation, not a Rayleigh type. This approach is handy for the parallel panel case or the complex problem. One example is shown.

Comparison With Experiment

Tests were conducted with a rectangular tank constructed with a rugged frame, to which were attached stiff nontest panels of 1/4-in. thick aluminum and a plexiglass panel 1-in. thick for viewing. Thinner flexible aluminum test panels, $0.063 \times 10 \times 16$ in., were configured as ends or bottoms. Care was taken to insure that negligible static bowing occurred during the tests. Tank length was varied from 3 to 24 in., and fluid depths varied from 0 to 16 in. for the end panels tests. The top was vented to the air. A bottom panel was tested for 0-8 in. of fluid depth, using the 10×16-in. end panel with the tank turned on end and vented at the opposite end.

Figure 3 compares experimental and theoretical frequencies (Rayleigh-Ritz) vs fluid height for a flexible end panel of size 10×6 in. for a tank length of 24 in. Fixed edge conditions were considered in theory to duplicate the conditions in the experiment. The first three experimental panel modal frequencies are shown. Both methods show good agreement with experiment for fluid levels above 20% full, with the BCS being slightly the better. Neither method shows as good a correlation with the test data at fluid heights of 10-15% because of an acoustic resonance at those levels (see x on figure). This is due to the panel modes coupling with the acoustic resonance at these fluid levels.

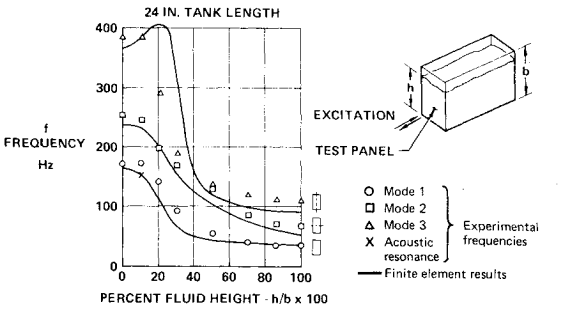

Fig. 5 Comparison of experimental and theoretical finite element frequencies vs fluid height for the flexible end panel.

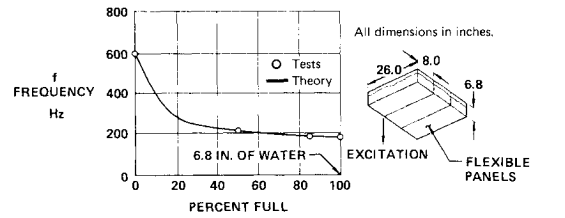

Fig. 6 Frequency variation vs fluid depth for wet torque box skins.

Figure 4 compares the experimental and theoretical frequencies vs fluid height for the flexible bottom panel. The first three experimental modal frequencies for the panel are shown, as are theoretical frequencies obtained using the BCS fluid velocity profiles in the Rayleigh-Ritz Method. Excellent correlation is shown. The mode shapes and node lines were accurately predicted by our method for both the end and side panels. Note that the bottom panel evidences more effect of fluid height on frequencies than does the side panel. However, greater distortions in frequency trends are shown by the end panel. The end panels exhibit markedly changed mode shapes for the lower fluid heights, while the bottom panel evidences only slightly distorted mode shapes for all fluid heights. This shows a significant influence on panel flutter as discussed below.

Figure 5 compares frequencies calculated in a preliminary finite element model and the measured frequencies for the end panel for the 24-in. tank length. Velocity profiles at each panel element were based on averaging adjacent grid point velocities. Good correlation is shown for the first mode, especially at the higher fluid levels, and for the second mode generally. Correlation at the lower fluid levels is not as good as for the higher levels because the fluid finite elements became too large to accurately define the fluid masses. More elements are needed, or a finer grid is needed at the lower levels. Likewise, mode 3 correlation would be improved from a more detailed modeling and a more accurate use of grid point velocities.

Applications

Formative applications of fluid-structure interaction were made in the areas of fatigue, flutter, and hydraulic ram, with key details of the former two presented below.

Fatigue

Since wetted panels can exhibit sharply reduced frequencies without significant increases in damping, and because of the more intense excitation at the lower frequencies, it was believed that fatigue life could be reduced. Furthermore, the influence of environmental vibration simulated by moving base excitation was believed to produce higher stresses at high fluid levels, further reducing fatigue life. Thus, for an example of a thicker skin which normally has good fatigue resistance dry but which would exhibit adequate effects of fluid-structure to warrant deeper study, we selected a torque-

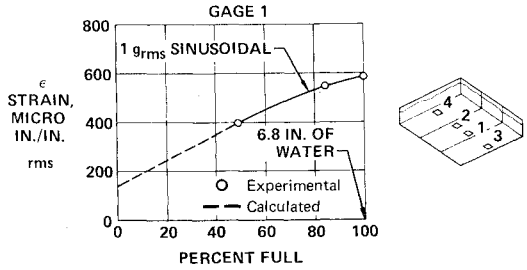

Fig. 7 Strain variation at box skin resonance vs fluid depth.

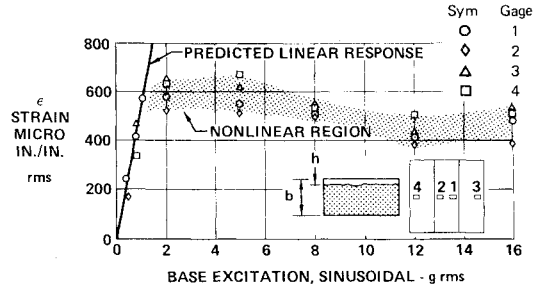

Fig. 8 Strain response of box lower skin panels vs excitation level, full case.

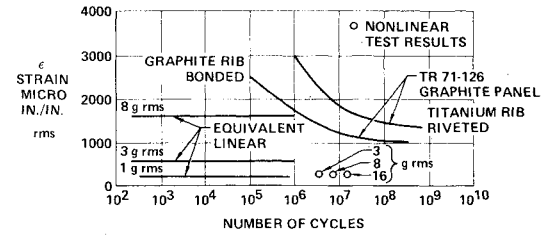

Fig. 9 Life cycle evaluation of box lower skin panel, full fuel case.

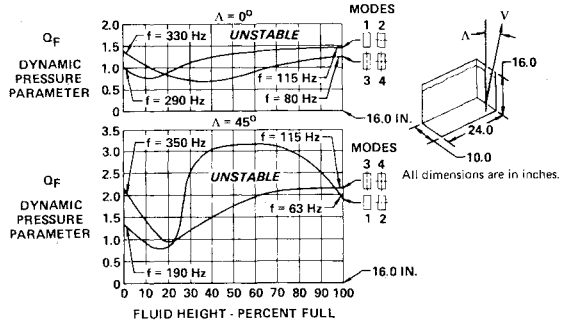

Fig. 10 Panel flutter results for airflow on end panel of tank.

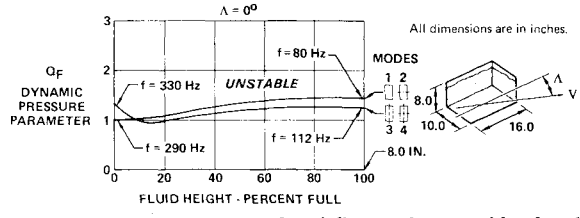

Fig. 11 Panel flutter results for airflow on bottom side of tank.

box section of a composite wing on an advanced aircraft (see Fig. 6). A section 26 × 26 × 6.8 in. was constructed with composite skins and with two composite interior spars with sinusoidal webs attached. It is enclosed by two metal exterior spars and two metal ribs. The composite skins were 1/4-in. thick graphite epoxy. Moving base excitation was used to determine basic vibration properties and for the fatigue study. Figure 6 shows the variation of first mode frequency vs fluid depth. This shows a 3/1 drop over the dry state. This is considerable for this thickness, but it is predicted closely by our method as shown in the figure. Figure 7 shows the maximum strains ϵ measured and calculated at resonance at 1 g rms sinusoidal excitation level. Similar results were obtained using narrow band random input. This shows a range of strains ϵ from 180–575 μ as the fluid height varied from empty to full. This is a growth of nearly 4/1 over the dry case, and is rather surprisingly large for such a thickness. This could add a significant strain level to the statics-only design value (3000 μ) in our general usage. Consider also that the strains would be more severe for a thinner panel, thus posing a more stringent influence on design in that case.

Figure 8 shows a plot of panel strain response vs excitation levels for the full case. A linear region was evidenced for excitation below 1 g rms and closely predicted. For excitation of 2 g's rms or greater, a nonlinear response region was found where strain growth was inhibited. This same type of result was obtained with narrow band random input using a bandwidth sufficiently wide enough to excite the basic panel resonance at all times. A check on the life cycle behavior was conducted using narrow band random input, with test times and durations of: 3g's rms for 8 h, 8 g's rms for 6 h, and 16 g's rms for 4 h. No failure was encountered with the results summarized as shown in Fig. 9. Here the measured test strains were plotted at the test times and fall well below the strain-to-failure curves ($\epsilon - N$) of TR-71-126 which are typical of our material. This life cycle is considerably longer than the life expected from linear response as shown in Fig. 9. Here, the linear response lines for 1, 3, and 8 g rms are shown, the latter intersecting the $\epsilon - N$ curves. The nonlinear relief shown here may not be representative of actual in-flight conditions. Effects such as static pressure and maneuver load may affect fluid dynamics and may not allow the nonlinear mitigations of strain rate growth. This is worthy of further study, and we are now looking into the problem.

Combined fatigue life reflecting statics and dynamic strain would be considerably different. It is obvious that thinner skins such as found in fuselage fuel cells may exhibit more critical conditions and thus may evidence failures. A number of instances do exist. One study[8] shows a case where fatigue life was not predicted by statics or low frequency analysis. Statics-only loads were increased considerably to match measured in-service failures. Inclusion of the fluid-structure interaction would have probably helped to bridge the differences between the statics-only approach and the actual fatigue producing load.

Panel Flutter

Fluid-structure interaction is envisioned to have a significant influence on panel flutter. The sharply reduced frequencies of wetted panels place them in close approximation to wing modes, thus posing a new type of flutter involving panel and wing modes. Panels separated by a fluid column can be interrelated by fluidic coupling; an example would be the upper and lower wing skins separated by wing fuel for a partial fuel condition in a climb or dive attitude. Also, the fluidic effects on modal frequency and mode shape vs fuel level in a tank will produce different panel flutter properties compared to the dry state. We have attempted to conduct a first-cut type of analysis of the latter case using our test tank panels. It was assumed that air could flow along either the flexible end or along the flexible bottom, while the fluid level of either case was varied. Simplified aerodynamics were employed to add insight. In this approach, the method of Zimmerman[9] was used as a starting point. The aerodynamic pressure was assumed proportional to the local slope, with a magnitude based on the Ackeret relationship for supersonic flow on one side of the panel. A Rayleigh-Ritz solution was used where the panel vibration modes at zero airspeed were

degrees of freedom. Our Rayleigh-Ritz vibration method was extended to include air load computations and flutter stability calculation.

Figures 10 and 11 show results of the studies using the first four vibration modes. Figure 10 shows the flutter results for flow along one end, with flow yaw angles of 0 and 45 deg relative to the vertical direction. A flutter dynamic pressure parameter Q_F is plotted vs fluid height for two mechanisms. Values of dynamic pressure equal to or above Q_F correspond to unstable conditions. The aerodynamics show skew symmetric coupling between pairs of modes, i.e., between modes 1 and 2, and modes 3 and 4; thus, two different boundaries result. Principally, one sees that the full and empty results are similar in Q_F but of different frequencies. This is due to similar frequency ratios, mode shapes, and mass coupling.

For intermediate fluid levels, the frequency separation, mass coupling, and modal distortion alter the flutter process considerably. Partial fluid levels are more stringent, and the critical modes switch. Figure 11 shows results for flow along the bottom, at zero yaw angle. This indicates considerably less influence of fuel effects than does the side panel. Thus, while the bottom panel is more strongly affected in terms of frequency shift vs fluid height, this shift is less distorted than those of the end panel, indicating less influence of frequency separation on flutter in this case. Likewise, model distortion and modal coupling are considerably smaller than for the end panel. We feel that this study should be pursued further with more comprehensive aerodynamics to substantiate the sensitivities noted here.

Conclusions

A description of the fluid-structural interaction in fuel cell cavities has been developed, including an accurate computational means for quantitative analyses. The process has shown to lead to major changes in structural vibration, giving rise to possible new problem areas not previously considered. Limited or exploratory examples were given to substantiate the ideas for application, and suggest that design considerations need to be expanded to compensate for the implications.

Acknowledgment

This work was sponsored by McDonnell Aircraft Company.

References

[1] Lamb, Horace, "On the Vibrations of an Elastic Plate in Contact with Water," Proceedings of the Royal Society of London, Series A, Vol. 98, 1920.

[2] MacNeal, R.H., "The NASTRAN Theoretical Manual," (Level 15.5), MSR-40, The MacNeal-Schwendler Corp., May 1974.

[3] Coppolino, R.N., "A Numerically Efficient Finite Element Hydroelastic Analysis," Vol. 1: *Theory and Results*, NASA CR-2662, April 1976.

[4] Kiefling, L. and Feng, G.C., "Fluid-Structure Finite Element Vibrational Analysis," *AIAA Journal*, Vol. 4, Feb. 1976, pp. 199-203.

[5] Kalinowski, A.J., "Fluid-Structure Interaction," *Shock and Vibration Computer Programs*, SVM-10, The Shock and Vibration Information Center, United States Department of Defense, 1975.

[6] Hunt, D.A., "A General Principle in Dynamic Response of Fluid Structure Interaction," *Journal of Applied Mechanics*, Dec. 1976.

[7] Hunt, D.A., "Discrete Idealization of an Incompressible Liquid for Vibration Analysis," *AIAA Journal*, Vol. 8, June 1970, pp. 1001-1004.

[8] Dumas, E., "Results of the F-4 Fuel Cavity Fatigue Test," ASD-ENFS TM 76-03, July 1976.

[9] Zimmerman, N.H. and Lemley, C.E., "Cavity Effect in Panel Flutter—Just How Significant?," *The Shock and Vibration Bulletin*, No. 40, Part 4, Dec. 1969.